JACS
JOURNAL OF THE AMERICAN CHEMICAL SOCIETY
Article
pubs.acs.org/JACS

Oxidation-Responsive and "Clickable" Poly(ethylene glycol) via Copolymerization of 2-(Methylthio)ethyl Glycidyl Ether

Jana Herzberger,[†,‡] Karl Fischer,[§] Daniel Leibig,[†,‡] Matthias Bros,[∥] Raphael Thiermann,[⊥] and Holger Frey*[,†,‡]

[†]Institute of Organic Chemistry, Johannes Gutenberg-University Mainz, Duesbergweg 10-14, 55128 Mainz, Germany
[‡]Graduate School Materials Science in Mainz, Staudinger Weg 9, 55128 Mainz, Germany
[§]Institute of Physical Chemistry, Johannes Gutenberg-University Mainz, Duesbergweg 10-14, 55128 Mainz, Germany
[∥]Department of Dermatology, University Medical Center of the Johannes Gutenberg-University, Langenbeckstrasse 1, 55131 Mainz, Germany
[⊥]Fraunhofer ICT-IMM, Carl-Zeiss-Str.18-20, 55129 Mainz, Germany

Supporting Information

ABSTRACT: Poly(ethylene glycol) (PEG) is a widely used biocompatible polymer. We describe a novel epoxide monomer with methyl-thioether moiety, 2-(methylthio)ethyl glycidyl ether (MTEGE), which enables the synthesis of well-defined thioether-functional poly(ethylene glycol). Random and block mPEG-*b*-PMTEGE copolymers (M_w/M_n = 1.05−1.17) were obtained via anionic ring opening polymerization (AROP) with molecular weights ranging from 5 600 to 12 000 g·mol^{-1}. The statistical copolymerization of MTEGE with ethylene oxide results in a random microstructure (r_{EO} = 0.92 ± 0.02 and $r_{MTEG\ E}$ = 1.06 ± 0.02), which was confirmed by *in situ* ^{1}H NMR kinetic studies. The random copolymers are thermoresponsive in aqueous solution, with a wide range of tunable transition temperatures of 88 to 28 °C. In contrast, mPEG-*b*-PMTEGE block copolymers formed well-defined micelles (R_h ≈ 9−15 nm) in water, studied by detailed light scattering (DLS and SLS). Intriguingly, the thioether moieties of MTEGE can be selectively oxidized into sulfoxide units, leading to full disassembly of the micelles, as confirmed by detection of pure unimers (DLS and SLS). Oxidation-responsive release of encapsulated Nile Red demonstrates the potential of these micelles as redox-responsive nanocarriers. MTT assays showed only minor effects of the thioethers and their oxidized derivatives on the cellular metabolism of WEHI-164 and HEK-293T cell lines (1−1000 μg·mL^{-1}). Further, sulfonium PEG polyelectrolytes can be obtained via alkylation or alkoxylation of MTEGE, providing access to a large variety of functional groups at the charged sulfur atom.

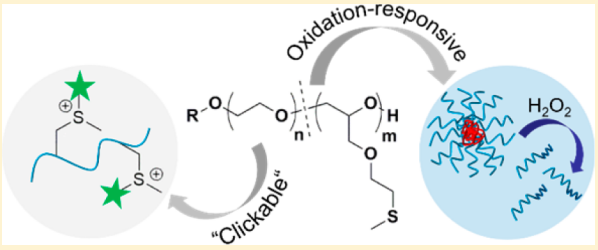

INTRODUCTION

In recent years, there has been an emerging interest in aliphatic thioether-functional polymers.[1] At first glance, thioethers may seem rather unreactive and unspectacular, particularly compared with their thiol or disulfide analogues, and thus have often been overlooked as a functional group by themselves. However, in contrast to regular ethers, the nature of sulfur provides the possibility to functionalize thioethers via oxidation, alkylation, and alkoxylation,[1−4] which can lead to interesting material properties. In the 1970s, Ringsdorf and co-workers demonstrated that oxidized poly[2-(methylsulfinyl)ethyl acrylate] and poly[2-(methylsulfinyl) methacrylate] can serve as polymeric resorption enhancing alternatives to low molecular weight DMSO.[5,6] Thirty years later, Hubbell, Tirelli, and co-workers recognized the potential of polythioethers as redox-responsive nanocarriers for inflammation targeting.[7] In the oxidative milieu of inflamed tissue, hydrophobic thioethers are oxidized to more polar sulfoxides or sulfones, leading to a change in the hydrophobic/hydrophilic balance with disassembly of the nanostructure. This remarkable work inspired the design of various oxidation-responsive nanocarriers based on thioether-functional polymers.[8−19] Additionally, the nucleophilicity of sulfides allows for sulfonium salt formation with alkyl halides, similar to the quaternization of amines. Deming and co-workers demonstrated the suitability of thioether moieties as precursors for a variety of stable, water-soluble, and highly functional polypeptide sulfonium derivatives, by click-type "quaternization" of poly(L-methionine).[3,4,20] Furthermore, their analogy to nitrogen-based polyelectrolytes inspired Long and co-workers to study sulfonium-functional PMMA derivatives as nonviral nucleic acid delivery agents.[21] Similar structures have also been investigated for siRNA complexation, confirming their high potential as drug delivery vehicles in biological environments.[22]

For biomedical applications, hydrophobic thioethers are often combined with poly(ethylene glycol) (PEG) as a hydrophilic block to provide aqueous solubility. PEG is a

Received: May 3, 2016
Published: July 2, 2016

DOI: 10.1021/jacs.6b04548
J. Am. Chem. Soc. 2016, 138, 9212−9223

Scheme 1. Anionic Ring Opening Polymerization (AROP) of MTEGE with EO or with mPEG as Macroinitiator, Yielding Random and Block Copolymers[a]

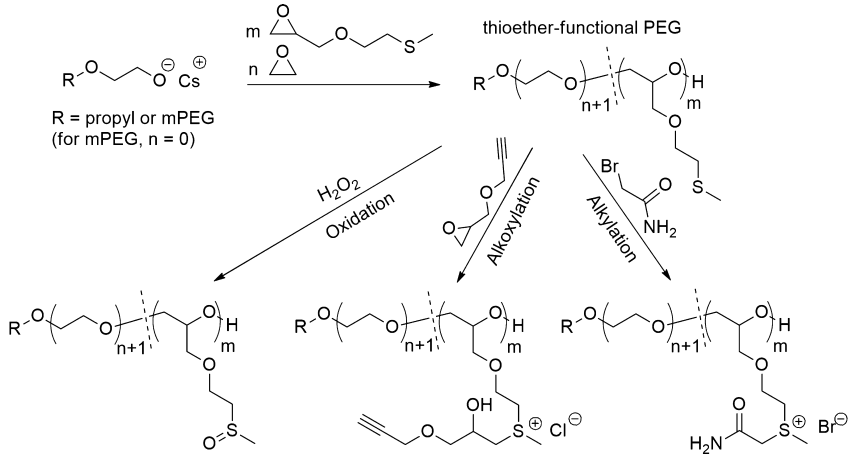

[a]Functionalization can be performed via oxidation, alkoxylation or alkylation.

highly water-soluble, biocompatible polyether with low immunogenicity, antigenicity, and toxicity.[23] However, for most of the strategies mentioned above, the nature of the thioether block differs strongly from PEG or is based on step-growth polymerization,[17,19] which is accompanied by broad molecular weight distributions.

Here, we present the synthesis of a novel epoxide building block, 2-(methylthio)ethyl glycidyl ether (MTEGE), which is broadly applicable to generate thioether functional PEGs via anionic ring opening polymerization (AROP) (Scheme 1).

We believe that MTEGE represents a useful alternative to episulfide/propylene sulfide, acrylate-based monomers or thiol−ene click chemistry, because it leads to well-defined polymers with a mere polyether backbone and *S*-methyl moieties as side chains. Most important, AROP of epoxides is a well-established industrial process. To date, similar structures have only been reported by postpolymerization modification of polyepichlorohydrin with sodium alkanethiolates.[24] Additionally, we demonstrate the suitability of thioether-PEGs for (1) oxidation-responsive structures and (2) functional sulfonium-PEG polyelectrolytes (Scheme 1).

EXPERIMENTAL PROCEDURES

Monomer Synthesis. 2-(Methylthio)ethyl glycidyl ether was synthesized in analogy to *N*,*N*-diisopropylglycidylether.[25] 2-(Methylthio)ethanol (1 equiv, 10 mL) was introduced to a round-bottom flask, and crushed sodium hydroxide pellets (1 equiv, 4.6 g) were added. The mixture was cooled to 0 °C, and epichlorohydrin (2 equiv, 18 mL) was added dropwise, followed by vigorously stirring for 48 h. Afterward, the mixture was placed in a centrifuge (15 min, 4500 rpm), and the organic phase was collected and dried over $MgSO_4$. The product was purified via fractionated vacuum distillation (p = 0.006 mbar, T_b = 60 °C). Repeated distillation resulted in yields of 50−60%. ρ (23 °C) = 1.10 g·mL^{-1}. ^{1}H NMR ($CDCl_3$, 400 MHz, δ): 3.78 (dd, 1H, ring−C$H_{2,a}$O-, J = 11.6, 2.9 Hz); 3.77−3.58 ppm (m, 2H, -OCH_2CH$_2$); 3.40 (dd, 1H, ring−C$H_{2,a}$O-, J = 11.6, 5.9 Hz); 3.15 (ddt, 1H, CH_{ring}, J = 5.7, 4.1, 2.8 Hz), 2.79 (dd, 1H, C$H_{2b,ring}$, J = 5.0, 4.2 Hz); 2.69 (t, 2H, −CH_2S, J = 6.7 Hz); 2.61 (dd, 1H,C$H_{2a,ring}$, J = 5.0, 2.7 Hz); 2.14 (s, 3H, −CH_3,). ^{13}C NMR ($CDCl_3$, 100 MHz, δ): 71.73 (ring-CH_2O−), 70.79 (-OCH_2CH$_2$), 50.93 (CH_{ring}), 44.32 (C$H_{2,ring}$), 33.67 (−CH_2S), 16,19 (−CH_3). FDMS m/z: [M$^+$] calcd for $C_6H_{12}O_2S$, 148.06; found, 148.2. All information on additional reagents, methods, and reaction conditions are detailed in the Supporting Information.

RESULTS AND DISCUSSION

Monomer Synthesis, Polymerization of MTEGE and Copolymerization with EO, Characterization, and Thermal Properties. *Monomer Synthesis.* MTEGE was synthesized in a one-step procedure starting from epichlorohydrin and 2-(methylthio)ethanol (both commercially available) (Scheme 2), in analogy to the literature known *N*,*N*-diisopropyl ethanolamine glycidyl ether (DEGE).[25]

Scheme 2. Synthesis of the Thioether Functional Epoxide Monomer 2-(Methylthio)ethyl Glycidyl Ether (MTEGE)

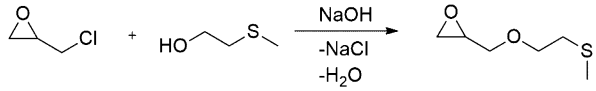

Purification was performed via repeated fractionated distillation under reduced pressure, lowering the overall yield to 50−60%. However, unreacted reagents can be recollected. Note that column chromatography (silica and aluminum oxide) should be avoided due to occurring side reactions, most likely due to catalyzed ring-opening of the epoxide by the thioether unit. Detailed characterization by ^{1}H, ^{13}C, and 2D NMR is given in the Supporting Information (Figures S1−S4).

PEG-ran-PMTEGE and mPEG-b-PMTEGE Copolymers and PMTEGE Polymers. The thioether-functional epoxide MTEGE can be polymerized via anionic ring opening polymerization (AROP) in a one-step procedure. Here, we synthesized multithioether functional PEG with random or block-type structures by either (i) statistical copolymerization of MTEGE with EO (PEG-*ran*-PMTEGE) or (ii) initiation of MTEGE with mPEG (mPEG-*b*-PMTEGE) (Scheme 1). Further, PMTEGE homopolymer was successfully prepared. All polymers and copolymers show monomodal distributions and narrow PDIs (1.05−1.17) with molecular weights in the range of 5000−12000 g·mol^{-1} (Figure 1, Table 1). The block copolymers show a clear shift to smaller elution volumes (higher molecular weights) with increasing MTEGE units, compared with the macroinitiator mPEG-5000 (Figure 1, right).

The molecular weights of the block copolymers were found to be slightly lower than anticipated (Table 1). Chain transfer

DOI: 10.1021/jacs.6b04548
J. Am. Chem. Soc. 2016, 138, 9212−9223

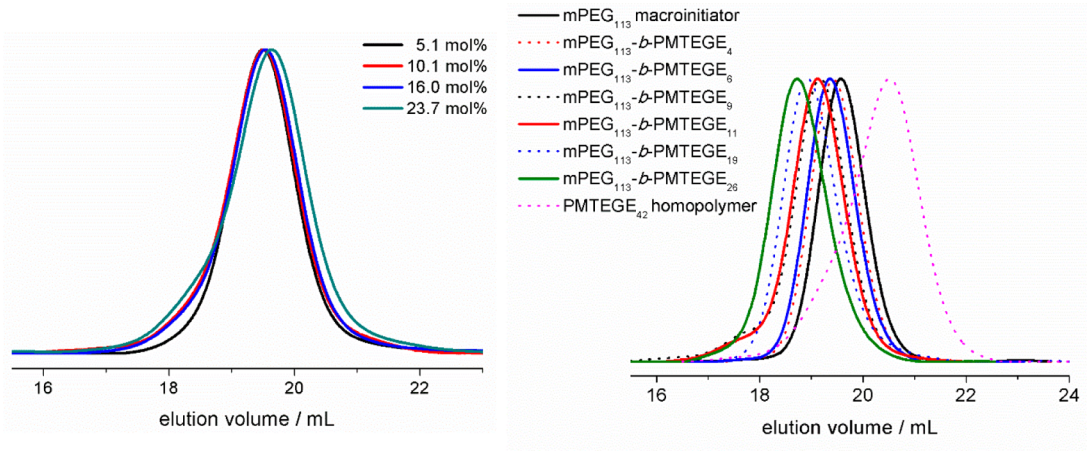

Figure 1. SEC elution traces (DMF, PEG standard, RI detection) of random PEG-*ran*-PMTEGE copolymers (left) and $mPEG_{113}$ macroinitiator, mPEG-*b*-PMTEGE block copolymers, and PMTEGE homopolymer (right).

Table 1. Characterization Data for the Series of Random PEG-*ran*-PMTEGE, mPEG-*b*-PMTEGE Block Copolymers, and mPEG and PMTEGE Homopolymers

sample[b]	MTEGE[a]	MTEGE[b]	M_n[b] / g·mol^{-1}	M_n[c] / g·mol^{-1}	PDI[c]	T_g[d] / °C	T_m[e] / °C	ΔH[f] / J·g^{-1}	T_c[g] / °C
$mPEG_{113}$	0	0	5000	4700	1.05	−53	64	186	
PEG_{150}-*ran*-$PMTEGE_8$	5	5.1	7800	4900	1.06	−61	35	82	88
PEG_{178}-*ran*-$PMTEGE_{20}$	10	10.1	10800	4900	1.15	−64	22	40	60
PEG_{137}-*ran*-$PMTEGE_{26}$	15	16.0	10000	4700	1.15	−64	7	30	46
PEG_{135}-*ran*-$PMTEGE_{42}$	25	23.7	12200	4560	1.17	−63			28
$mPEG_{113}$-*b*-$MTEGE_4$	4.2	3.4	5590	4980	1.08	−57	57	150	
$mPEG_{113}$-*b*-$MTEGE_6$	5.0	5.0	5890	5130	1.08	−58	56	142	
$mPEG_{113}$-*b*-$PMTEGE_9$	8.1	7.4	6330	5890	1.15	−58	55	125	
$mPEG_{113}$-*b*-$PMTEGE_{11}$	9.6	8.9	6630	5820	1.09	−59	55	123	
$mPEG_{113}$-*b*-$PMTEGE_{19}$	15.0	14.4	7810	5940	1.10	−61	53	109	
$mPEG_{113}$-*b*-$PMTEGE_{26}$	20	18.7	8850	6840	1.09	−62	51	91	95
$PMTEGE_{42}$	100	100	6330	3300	1.14	−62			*h*

[a]Targeted comonomer content. [b]Comonomer content determined via ^{1}H NMR spectroscopy. [c]Determined via SEC measurements (DMF, RI signal, PEG standard). [d]Glass transition temperature. [e]Melting temperature. [f]Melting enthalpy. [g]Cloud point temperature determined via turbidity for c = 5 mg·mL^{-1}. [h]Insoluble.

to the monomer via proton abstraction can occur, which is a common side reaction for glycidyl ethers.[26] This leads to the formation of new initiating species, which generates homopolymer impurities and lowers the targeted molecular weight. However, side products were easily removed via precipitation of the block copolymers into diethyl ether (Figure S5). Note that no double bonds were detected for the random copolymers and proton abstraction can be excluded. A slight discrepancy of the targeted comonomer content might be due to small differences in measuring liquid EO.

Number-averaged molecular weights were determined from ^{1}H NMR spectra, referring all signals to the resonance of the initiator (Figure 2, Figures S6 and S7). The slight discrepancy between M_n obtained by NMR and SEC is caused by the hydrophobic thioether side chains, leading to a different hydrodynamic volume of PEG−PMTEGE (co)polymers compared with PEG (SEC in DMF, PEG standards). This trend is most distinct for the random PEG-*ran*-PMTEGE copolymers and is frequently observed for multifunctional PEGs.[27−29] EO/MTEGE ratios were also calculated from ^{1}H NMR spectra comparing the signal of the methyl group (−SCH_3) at 2.15 ppm to the polyether backbone signal at 3.4−3.8 ppm (Figures 2 and S7). Overall, ratios were varied from 3 to 24 mol %, yielding water-soluble polymers while preserving

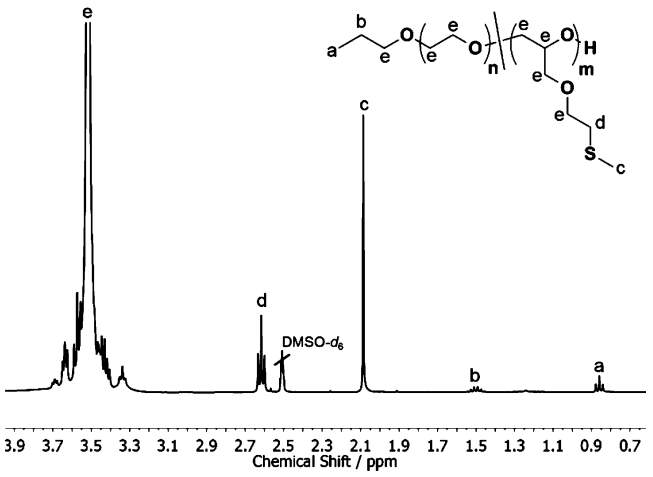

Figure 2. ^{1}H NMR spectrum (400 MHz, DMSO-d_6) of PEG-*ran*-PTMEGE with 5.1 mol % MTEGE.

PEG's outstanding properties and increasing its functionality (Table 1). The PMTEGE homopolymer is water-insoluble but is soluble in THF, benzene, and DMSO. Detailed ^{1}H and ^{13}C NMR characterization of the block and homopolymers are shown in the Supporting Information (Figures S6−S8).

DOI: 10.1021/jacs.6b04548
J. Am. Chem. Soc. 2016, 138, 9212−9223

To gain further information about the resulting microstructure of PEG-*ran*-PMTEGE, we monitored the copolymerization of EO and MTEGE in a vacuum sealed NMR tube. Both monomers are consumed constantly throughout the polymerization, with full conversion after 10 h (Figure 3 (bottom) in DMSO-d_6 at 40 °C). Measurements revealed random copolymerization of MTEGE and EO with reactivity ratios of r_{EO} = 0.92 ± 0.02 and r_{MTEGE} = 1.06 ± 0.02 and a product of $r_{EO} \times r_{MTEGE}$ = 0.98. The values were determined from Figure 3 (top) by applying a nonterminal model of chain copolymerization recently introduced by Lynd and co-workers.[30] We propose that the slightly higher reactivity of MTEGE results from both an increased coordination to the cesium counterion and an increased Lewis basicity of the epoxide ring compared with EO, as reported for other glycidyl ethers.[31] See the Supporting Information for characterization details (Figures S9 and S10).

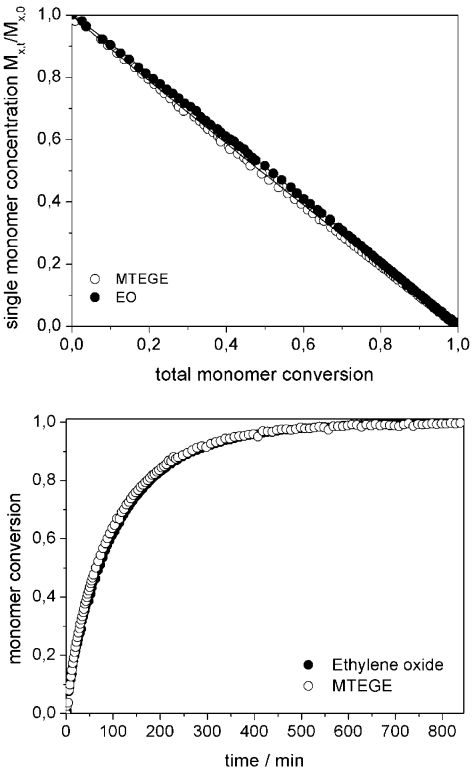

Figure 3. (top) Single monomer concentration versus total monomer conversion. Lines represent fits to the experimental data using the nonterminal model of chain copolymerization, proposed by Lynd and co-workers.[30] (bottom) Monomer conversion versus time. Statistical copolymerization was performed in DMSO-d_6 at 40 °C with the initial mole fractions n_{EO} = 0.585 and n_{MTEGE} = 0.415.

Inverse gated ^{13}C triad analysis further substantiates random microstructure of the copolymers. For simplicity, EO repeating units were abbreviated with E and MTEGE units with S, whereas a and b denote the methylene and methine carbon atom, respectively. Figure 4 illustrates an enlargement of the characteristic region of the S_b signal of PMTEGE homopolymer, mPEG-*b*-PMTEGE block copolymer, and various random copolymers. Focusing on the random copolymers, additional triads occur with increasing MTEGE content (E−S_b−S, S−S_b−E and S−S_b−S) while the intensity of the E−S_b−E triad leads to the most prominent signal for all compositions.

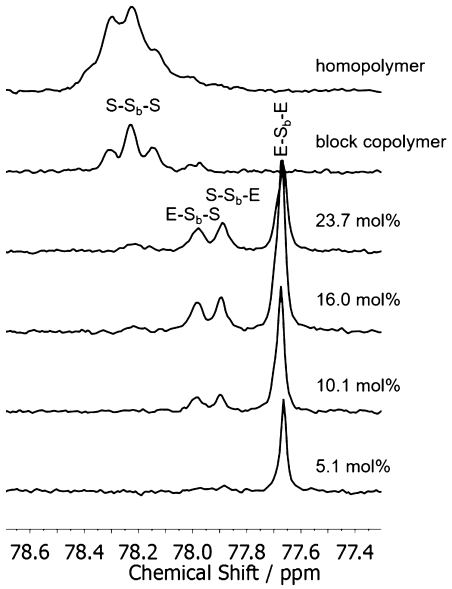

Figure 4. Enlargement of the IG ^{13}C NMR spectra (DMSO-d_6, 100 MHz) of PMTEGE homopolymer, mPEG-*b*-PMTEGE block copolymer, and various PEG-*ran*-PMTEGE copolymers, displaying the characteristic region of the S_b signal.

As expected, the E−S_b−E triad is absent for the block and homopolymer.

The region of EO centered triads is shown in Figure S11. Note that we refrained from assigning detailed triads in this region, due to a strong overlap of the EO- and S_a-centered triads with the signals of the MTEGE side chain (see also Figure S8). Nevertheless, the random copolymers possess more complex spectra than the block- and homopolymer, supporting the random microstructure.

The difference between random and block structures is also reflected by their thermal properties in bulk (Table 1). PEG itself is a highly crystalline polymer with a melting temperature approaching 65 °C when molecular weights exceed 2000 g·mol^{-1}.[32,33] Randomly distributed MTEGE units along the PEG backbone strongly inhibit its crystallization, leading to a significant decrease of the melting temperature and enthalpy with increasing MTEGE content. For example, only 5.1 mol % MTEGE is required to cause a drop in the melting temperature by 30 °C. Completely amorphous structures are detected when 23 mol % MTEGE is present. In contrast, for $mPEG_{113}$-*b*-$PMTEGE_n$, only a marginal influence of the MTEGE amount on the melting temperature and enthalpy of the PEG block was detected (Table 1). In this case, the block structure still allows PEG chains to align and crystallize. As expected, the atactic PMTEGE homopolymer is fully amorphous with a T_g of −62 °C. For the random copolymers, glass transition temperatures are in the range of −61 to −64 °C, similar to other multifunctional PEGs bearing nonpolar side groups.[34] Interestingly, we only detected one T_g for all block copolymers. This suggests rather poor phase separation due to the structural similarity of both blocks and the relatively short PMTEGE block.

Properties in Aqueous Solution. For future biomedical applications, it is important to understand the behavior of thioether-functional PEG copolymers in aqueous solution and to determine potential self-assembly and aggregation. Random PEG-*ran*-PMTEGE copolymers with MTEGE ratios of 5−24

DOI: 10.1021/jacs.6b04548
J. Am. Chem. Soc. 2016, 138, 9212−9223

mol % are water-soluble at room temperature, but turbid solutions are observed when samples are heated to a specific temperature. This so-called "thermoresponsiveness" is a common feature of multifunctional PEGs that bear hydrophobic units distributed along the polymer backbone, rendering them attractive for drug delivery applications.[28,35] PEG itself is fully water-soluble up to ~100 °C, due to the specific bond distance of its oxygen atoms, which allows for beneficial hydrogen bonding with water.[36] The incorporation of hydrophobic moieties leads to a decrease of both the number of water molecules bound to PEG and their configurational entropy; the latter results in a large entropy gain associated with their release, and therefore in an entropy-driven coil collapse upon heating. Polymers that exhibit phase transitions slightly above body temperature are interesting for medical applications such as therapeutic hypothermia.

With the incorporation of hydrophobic MTEGE units, one can tailor the aqueous solubility of PEG-*ran*-PMTEGE between 88 and 28 °C (5.1−23.7 mol %), as determined by turbidity measurements (Table 1, Figure 5). From Figure 5, one can conclude that MTEGE ratios between 16 and 20 mol % would be beneficial to cover the range near human body temperature. Repeated heating/cooling cycles show sharp phase transitions, complete reversibility, and little to no hysteresis (Figure S12). In contrast, the described mPEG-*b*-PMTEGE block copolymers with molar fractions of MTEGE below 14 mol % show no cloud point temperatures in the range of 0−100 °C at concentrations of 5 mg·mL^{-1}. Only mPEG$_{113}$-*b*-PMTEGE$_{26}$, the block copolymer with the highest amount of MTEGE, reveals a cloud point of 95 °C. In analogy to PEG-*co*-polysulfides and PEG-*b*-poly(butylene oxide) diblocks, block copolymers of mPEG$_{113}$-*b*-PMTEGE$_n$ with $n \geq 9$ show micellar gelation in water at high concentrations (20 wt %) at 25 °C.[16,37] In contrast, no gelation is observed for random copolymers, and the solutions turn opaque when heated.

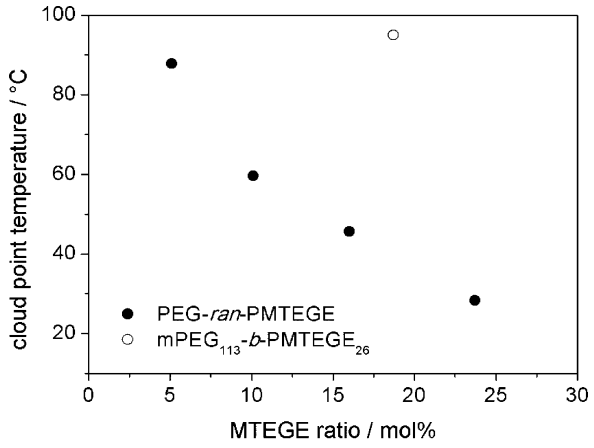

Figure 5. Cloud point temperatures plotted versus MTEGE content of PEG-*ran*-PMTEGE copolymers (solid spheres) and mPEG$_{113}$-*b*-PMTEGE$_{26}$ (hollow spheres). Error margins have been calculated from the standard deviation of the averaged values and are less than 1 °C.

These results suggest that mPEG-*b*-PMTEGE block copolymers exhibit completely different aggregation behaviors in water in comparison to their random counterparts.

To further elucidate their unique solubility behavior in water, we conducted dynamic light scattering (DLS) measurements. For the PEG-*ran*-PMTEGE copolymers, polydisperse samples at room temperature were observed, with the occurrence of unimers and larger aggregates. This can be attributed to a temperature-dependent association of PEG-*ran*-PMTEGE copolymers, already at temperatures below their respective cloud point (data not shown). Similar results were reported for other thermoresponsive polymers.[38−43]

In contrast to the random copolymers, block copolymers showed no strong thermoresponsiveness, suggesting well-defined self-assembly in water. We first conducted DLS in methanol, to ensure monomodal samples and to evaluate their respective hydrodynamic radii. For all samples, pure unimers were detected, showing an increase in the hydrodynamic radius with increasing MTEGE block length (Table S1). Intriguingly, when the block length of the hydrophobic block exceeds 6 units, aggregation of the block copolymers is forced by switching to an aqueous solution. For mPEG-*b*-PMTEGE$_n$ with the longest hydrophobic block (n = 26 MTEGE units), a micelle size of roughly 30 nm can be observed with a low polydispersity (the largest particles being nearly monodisperse (μ_2 < 0.05)). From Figures S13−16, one can observe that all experimental diffusion coefficients show no scattering angle dependency and low polydispersities as typical for micellar like

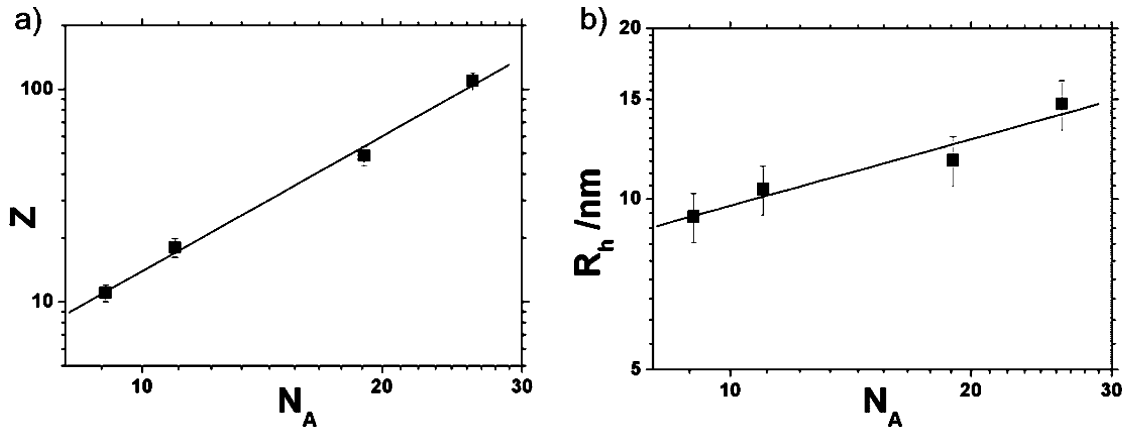

Figure 6. Scaling behavior of the aggregation number Z (a) and the hydrodynamic radius R_h (b) for mPEG$_{113}$-*b*-PMTEGE block copolymers with the block length N_A, as deduced from the polymer/low molar mass micellar aggregation theory by Förster et al.; exponents from theory 2 and 0.4, respectively, experimentally found 2.1 and 0.39, respectively.

DOI: 10.1021/jacs.6b04548
J. Am. Chem. Soc. 2016, 138, 9212−9223

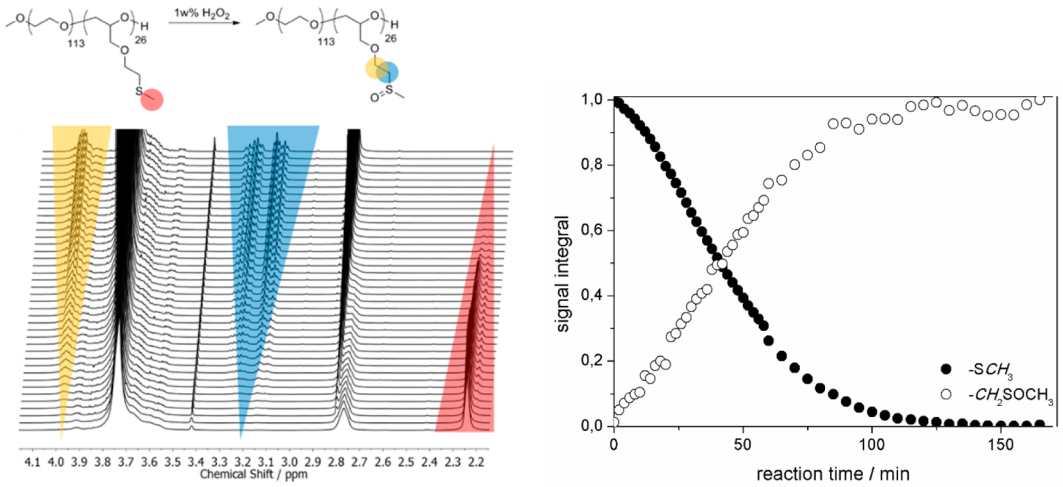

Figure 7. Selection of time-resolved ^{1}H NMR spectra (buffered D_2O, 400 MHz) of the oxidation of mPEG$_{113}$-*b*-PMTEGE$_{26}$ with 1 wt % H_2O_2 (left). Signal integral of the methyl signal (−SCH_3) and methylene signal (−CH_2SOCH_3) plotted versus reaction time for the oxidation of mPEG$_{113}$-*b*-PMTEGE$_{26}$ with H_2O_2 in buffered D_2O at 310 K (right).

assemblies. Fluorescence spectroscopy (with pyrene as a probe) was conducted to determine the CMC of all block copolymers, which still show self-assembly at a concentration of 1 g·L^{-1}, and CMCs are listed in Table S1. The CMCs range from 100 to 1.5 mg·L^{-1} for mPEG$_{113}$-*b*-PMTEGE$_n$ with n = 9 and 26, respectively. These are in the range of values reported for PEG-*b*-poly(butylene oxide) diblock copolymers with similar hydrophobic block length[44,45] and other PEG-based diblocks.[46,47]

To gain further insight into the topology and aggregation number of the samples, we performed static light scattering (SLS) (Figure S17−18). Measurements in methanol and water prove that all samples show no angular dependency of the scattering intensity, indicating a radius of gyration (R_g) below 10 nm (Table S1). Hence, for the block copolymers with 19 and 26 MTEGE units, the ρ-ratios ($\rho \equiv$ "R_g/R_h" = $\langle R_g^2 \rangle_z^{1/2} / \langle 1/R_h \rangle_z^{-1}$) are below 1, which is in accordance with the micellar hypothesis ($\rho_{\text{hard-spheres}}$ = 0.775).[48] From these results, we calculated the aggregation number Z (K_c/R in methanol versus K_c/R in water, see Supporting Information for details) (Table S1). One can observe a strong increase in Z with increasing MTEGE block length, also reflected by the increase of the hydrodynamic radius. Correspondingly, mPEG-*b*-PMTEGE block copolymers follow the scaling laws developed by Förster et al. for block copolymer micelles, which substantiates the micellar hypothesis.[49] This is clearly reflected by Figure 6, which summarizes the experimental results in agreement with the scaling behavior introduced by Förster et al.

The aggregation number Z depends on the block length N_A of the hydrophobic block with an exponent of 2 (expt 2.1), whereas the hydrodynamic radius (R_h) scales with the exponent of 0.4 on N_A (expt 0.39), both determined from double logarithmic representation of the experimental results described in detail in the Supporting Information.

CryoTEM measurements further show the formation of micelles and support the light scattering results (Figure S19). However, a detailed analysis was not possible owing to the poor contrast of PEG, leading to rather diffuse images. SANS or SAXS measurements would be necessary to gain further information on the copolymers' morphology and inner structure.

Oxidation Sensitivity. Thioether can be selectively oxidized to sulfoxide or sulfone moieties, which leads to a strong increase in their dipole moment.[2,50] Consequently, we expect a significant change in the polarity of PEG−PMTEGE copolymers upon oxidation of their MTEGE units, which should be reflected in their solubility properties in aqueous solution. To gain insight into the redox-sensitivity of MTEGE, we first monitored the oxidation of mPEG-*b*-PMTEGE with H_2O_2 in a NMR tube. Experiments were performed in D_2O (296 K) with 1 wt % H_2O_2 solution and in deuterated buffer solution (NaD_2PO_4/Na_2DPO_4; pD = 7.46;[51] 310 K), to predict the behavior at body temperature. Figure 7 shows an enlargement of the important section of ^{1}H NMR spectra for oxidation in buffered solution. The oxidized polymer species is observed after a few minutes by the formation of sulfoxide groups: First, the singlet of the methyl group (−SCH_3) at 2.25 ppm shows a splitting, indicating the occurrence of adjacent oxidized moieties, followed by complete disappearance. Meanwhile, a new singlet appears at 2.78 ppm, representing the methyl group next to the sulfoxide group (−SOCH_3). Further, the methylene group (−CH_2SCH_3) at 2.74 ppm shifts downfield to 3.07−3.27 ppm and a new resonance at 3.95 ppm appears, corresponding to the neighboring methylene group (−CH_2CH_2SOCH_3). The signal integrals of the decreasing methyl group (−SCH_3) and the increasing methylene group (−CH_2SOCH_3) versus time, are illustrated in Figure 7 (right). Oxidation at 310 K (buffer solution) shows full conversion after 2.5 h. In contrast, room temperature (296 K) slows down the reaction to 6 h (Figure S22). Figure S23 depicts the respective SEC traces, which show a slight shift to lower molecular weights after oxidation. We attribute this observation to the change in polarity, leading to a different hydrodynamic volume. Furthermore, ^{1}H NMR spectroscopy confirmed preservation of the polymer backbone (M_n and MTEGE ratio remain constant after oxidation and dialysis). Notably, only sulfoxide moieties were detected (via NMR) under both 296 and 310 K oxidation conditions, demonstrating that no further oxidation to sulfone groups occurs (Figures S24 and S25). These observations are in line with results reported by Tirelli and co-workers for poly(propylene sulfide) (PPS)[11,15] and others,[52] who reported the selective oxidation of thioethers moieties to sulfoxides by treatment with diluted H_2O_2.

DOI: 10.1021/jacs.6b04548
J. Am. Chem. Soc. 2016, 138, 9212−9223

Hypochlorite (OCl^-) is another biological oxidant generated during inflammatory processes[50] and was investigated as an additional oxidation agent. In contrast to hydrogen peroxide, treatment of mPEG-*b*-PMTEGE with 1 wt % sodium hypochlorite (NaOCl) solution leads to the formation of sulfone groups (Figure S26 and S27). Note that the occurrence of additional signals in the ^{1}H NMR spectrum and a broadening in the SEC trace might indicate side reactions, such as polyether cleavage (Figure S28). Analogous results were reported by Tirelli and co-workers for oxidation of poly(propylene sulfide).[11]

The changes in polarity from a nonpolar thioether to polar sulfoxide or sulfone units strongly influences the glass transition temperature. While $mPEG_{113}$-*b*-$PMTEGE_{26}$ shows a T_g of −61 °C, the emerging dipole−dipole interactions cause a T_g of −33 °C for the sulfoxide derivative ($mPEG_{113}$-*b*-$PMSOEGE_{26}$) and a further increase to −15 °C for the sulfone derivative ($mPEG_{113}$-*b*-$PMSO_2EGE_{26}$). Sarapas and Tew reported similar results for linear poly(ether-thioethers) and their oxidized counterparts.[52]

After understanding the oxidation process on a molecular level, the question arises of how oxidation of the thioether units influences the solubility behavior of PEG−PMTEGE copolymers in water. First, we followed the oxidation process of the random PEG-*ran*-PMTEGE copolymers via turbidity measurements. An aqueous PEG-*ran*-PMTEGE solution (5 mg·mL^{-1}) with a cloud point of 28 °C was tempered to 37 °C, and H_2O_2 solution was added under stirring. Directly after H_2O_2 addition, the transmitted laser light intensity increases, indicating the dissolution of aggregates due to increasing hydrophilicity of the oxidized species (Figure S29). After 8 min, an optically clear solution is observed with complete disappearance of aggregates. Similar results were reported by Chen and co-workers for linear poly(β-thioether ester).[17] Additionally, turbidity measurements of oxidized copolymers (PEG-*ran*-PMSOEGE) show fully water-soluble polymers, and no cloud points were detected.

In particular, we were interested in the behavior of mPEG-*b*-PMTEGE block copolymers in aqueous solution with H_2O_2 treatment to investigate their potential as oxidation-responsive nanocarriers.[1,12] To this end, we monitored the oxidation process of $mPEG_{113}$-*b*-$PMTEGE_{26}$ via DLS measurements in real-time. After the sample was heated to 37 °C, H_2O_2 was added to the sample, followed by fast mixing (c_{total} = 1 wt % H_2O_2). The temperature was kept at 37 °C during the measurement. Figure 8 shows the scattering intensity traces versus time on a logarithmic scale.

After a thermal equilibration period of about 5 min, a linear decrease of the scattering intensity time traces can be observed. We attribute this linear decay to the oxidation of the nonpolar sulfides to polar sulfoxide groups, which leads to micelles with lower aggregation numbers (decrease in scattering intensity) and the formation of unimers (Scheme 3). Similar observations are reported for the disassembly of other H_2O_2 responsive or pH sensitive micelles.[17,42,53] Unfortunately, it was not possible to detect "spike" free intensity traces for oxidation times exceeding 20 min. This may be caused by several effects; for example, formed oxygen bubbles may perturb the measurement, but also impurities of the H_2O_2 solution (not filtered) or the liberation of encapsulated impurities could lead to sudden increases in the scattering intensity. Huang et al. reported similar observations for DLS kinetic studies of acid sensitive polymeric micelles after complete hydrolysis. The authors observe bimodal distributions consisting of unimers and loose associates.[42] In analogy, Zhang et al. monitored the oxidation-responsiveness of phenylboronic acid-based polymers in DLS and described the formation of polymeric associates with a loose structure.[53]

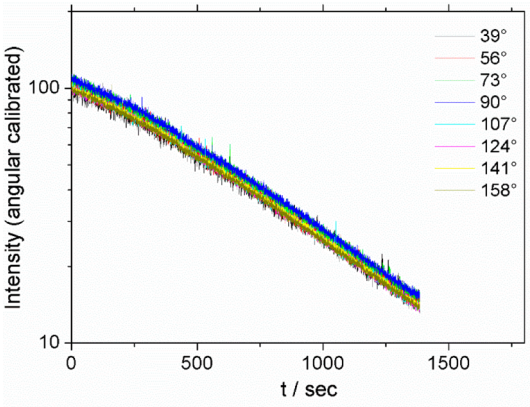

Figure 8. Angular dependent scattering intensity time traces (from multiangular goniometer setup) for *in situ* oxidation of $mPEG_{113}$-*b*-$PMTEGE_{26}$ (buffer solution, 37 °C, 1 wt % H_2O_2), shown on a logarithmic scale. The obvious change of the slope after 5 min is due to thermal equilibration.

To confirm our hypothesis of micelle dissociation and unimer formation, we performed DLS measurements of oxidized mPEG-*b*-PMSOEGE with 11 and 26 MSOEGE units. For both polymers, we detected pure unimers in water with hydrodynamic radii similar to their precursor polymers in methanol (Table S2). With the oxidation of MTEGE, the hydrophilic/hydrophobic balance of $mPEG_{113}$-*b*-$PMTEGE_n$ changes and leads to disassembly of the micelles into single polymer chains, as schematically shown in Scheme 3. Similar results were reported for the disassembly of PEG−polypropylene sulfide−PEG vesicles,[7] the dissolution of PEG-*b*-oligo(ethylene sulfide) fibrils,[54] and the oxidation of OEGylated poly-L-cysteine.[14]

Having demonstrated successful disassembly of micelles as a consequence of the treatment with hydrogen peroxide, we investigated their potential as responsive nanocarriers. Nile Red, a hydrophobic fluorescence dye, was encapsulated in the micelles, and their response to hydrogen peroxide (1 wt %) was studied.

Figure 9 shows the intensity of the fluorescence emission of Nile Red recorded over time after addition of H_2O_2 to a block copolymer solution ($c_{polymer}$ = 0.5 g·L^{-1}). Control measurements without H_2O_2 demonstrate stability of the micelles over the investigated time frame, and no significant loss of Nile Red is observed (Figure S30). With the addition of hydrogen peroxide, the fluorescence intensity of Nile Red decreases, indicating release of the dye due to its insolubility in aqueous solution. Complete release was detected after 1 or 2 h for $mPEG_{113}$-*b*-$PMTEGE_n$ with n = 11 and 26, respectively. For $mPEG_{113}$-*b*-$PMTEGE_{26}$, the intensity decrease follows a sigmoidal shape, which we attribute to an autoaccelerating character of the response in analogy to recent results by Tirelli and co-workers.[16] Significantly, the presented micelles respond faster to hydrogen peroxide than similar PEG (co)polysulfide (~8−24 h)[13,16] structures and PEG−poly(β-thioethers) (~7 h).[19] Although the biologically relevant concentration of H_2O_2 for inflamed tissue is in the range of ~100 μM,[55,56] this is a first demonstration of the response of polyether based polysulfide analogs. Detailed concentration dependence will be investigated

DOI: 10.1021/jacs.6b04548
J. Am. Chem. Soc. 2016, 138, 9212−9223

Scheme 3. Schematic of the Micelle Formation of mPEG$_{113}$-*b*-PMTEGE$_n$ Block Copolymers in Water, Followed by Disruption upon Treatment with H_2O_2[a]

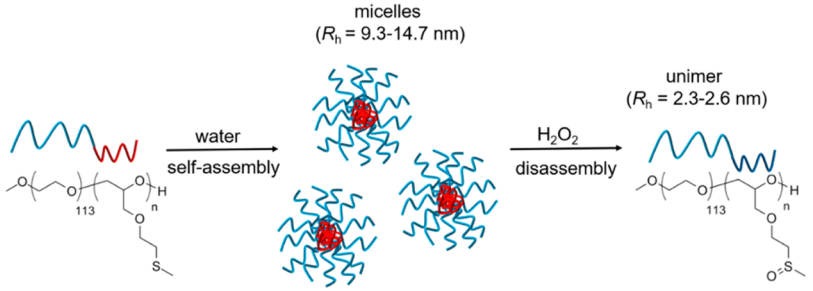

[a]The hydrodynamic radii were determined by DLS measurements (Table S1 and Table S2).

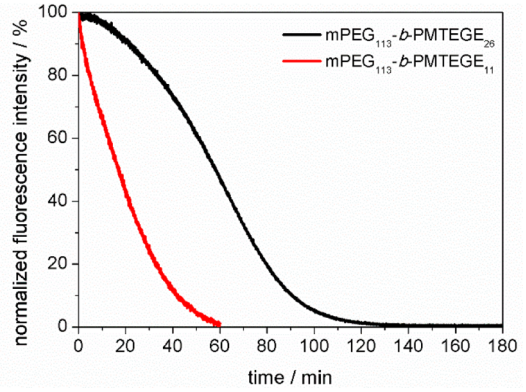

Figure 9. Intensity of fluorescence emission of Nile Red, monitored as a function of time after addition of H_2O_2 solution to a block copolymer solution ($c_{polymer}$ = 0.5 g·L^{-1}, $c_{H_2O_2}$ = 1 wt %, T = 25 °C).

in the future. Overall, we believe that mPEG-*b*-PMTEGE block copolymer architectures show potential as future redox-responsive drug vehicles and could be suitable for inflammation targeting.

Cell Viability Studies. PEG possesses excellent biocompatibility, including very low immunogenicity, antigenicity, and toxicity.[57] Low cytotoxicity is a crucial criterion for potential biomedical applications, and modification of PEG with thioether units may have an impact on these properties. Therefore, we conducted MTT assays to determine the effects of PEG−PMTEGE structures on the cellular metabolic activity of two different cell lines, HEK-293T cells (human embryonic kidney cells) and WEHI-164 cells (skin fibroblasts cells from mice), respectively. In a comparative study, mPEG itself and two samples of block and random PEG−PMTEGE copolymers with the highest amount of MTEGE were applied to seeded cells in concentrations of 1−1000 μg·mL^{-1}. MTT assays were performed after an incubation time of 24 h. Results are displayed in Figure 10. Focusing on the random copolymers

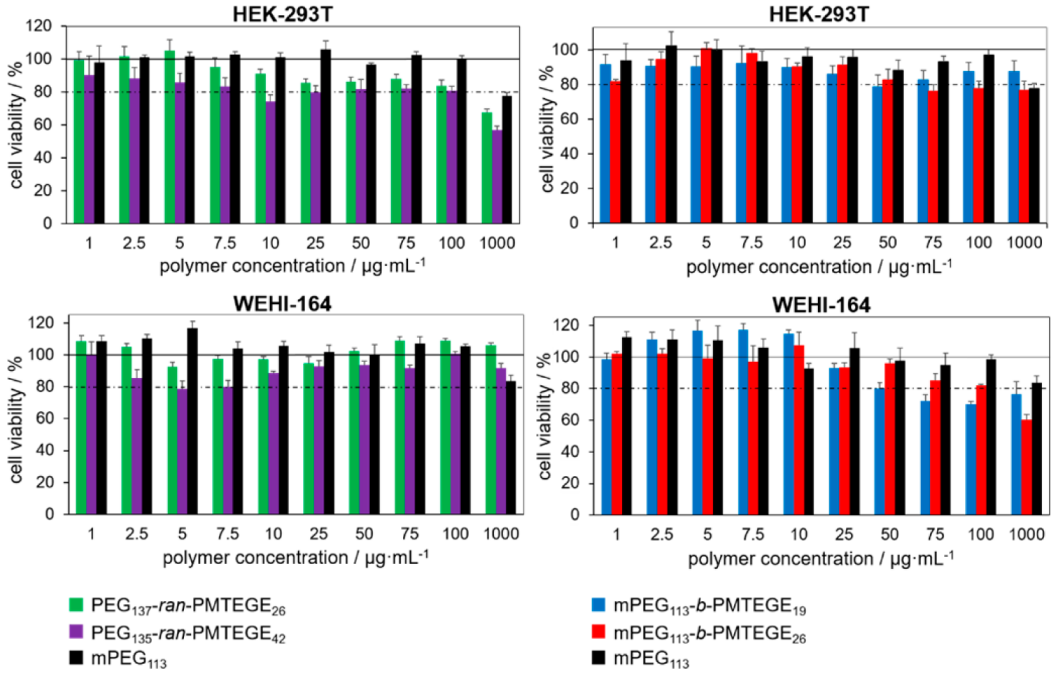

Figure 10. MTT assay of HEK-293T and WEHI-164 cells incubated with PEG−PMTEG random and block copolymers. For each type of polymer, copolymers with the highest amount MTEGE were tested. Results of mPEG$_{113}$ are shown for a better comparison. The metabolic activity of cells treated with 10% PBS buffer corresponding to the highest volume of copolymer solution added to samples was set to 100%. Graphs are representative of two independent experiments performed in triplicates. Data denote the mean ± SEM of triplicates.

DOI: 10.1021/jacs.6b04548
J. Am. Chem. Soc. 2016, 138, 9212−9223

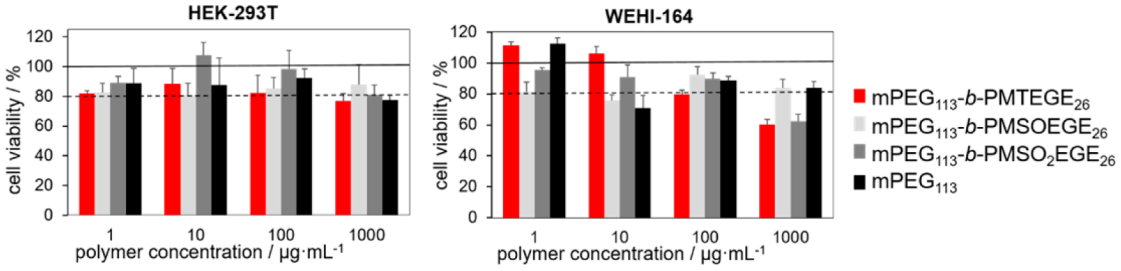

Figure 11. MTT assay of HEK-293T and WEHI-164 cells incubated with $mPEG_{113}$, $mPEG_{113}$-*b*-$PMTEGE_{26}$, and its oxidized derivatives, $mPEG_{113}$-*b*-$PMSOEGE_{26}$ (sulfoxide) and $mPEG_{113}$-*b*-$PMSO_2EGE_{26}$ (sulfone). The metabolic activity of cells treated with 10% PBS buffer corresponding to the highest volume of block copolymer tested was set to 100%. Graphs are representative of two independent experiments performed in triplicate. Data denote the mean ± SEM of triplicates.

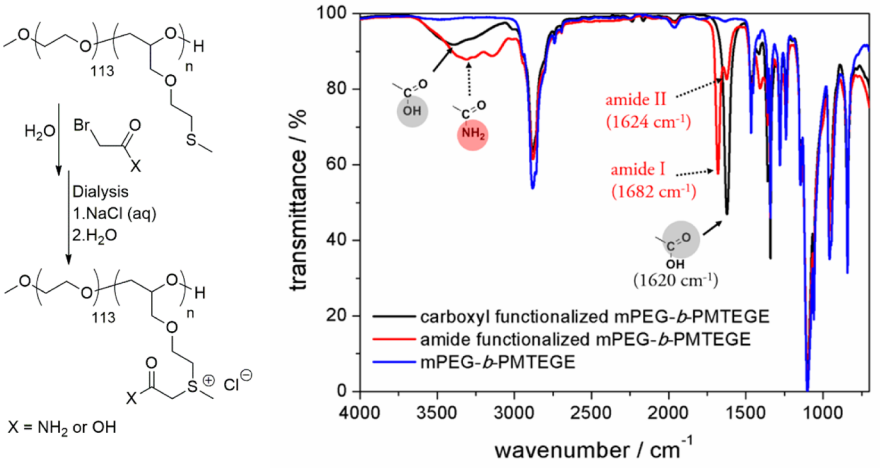

Figure 12. (left) Alkylation scheme. (right) FT-IR spectra of mPEG-*b*-PMTEGE (blue), carboxyl functionalized mPEG-*b*-PMTEGE (black), and amide functionalized block copolymer (red).

and HEK-293T cells, PEG_{137}-*ran*-$PMTEGE_{26}$ with 16 mol % MTEGE affected the metabolic activity by less than 20% up to rather high concentrations of 100 $\mu g \cdot mL^{-1}$. With an increase of MTEGE to 23.7 mol %, which corresponds to 51 wt % MTEGE, cellular metabolic activity is slightly reduced. For a concentration of 1000 $\mu g \cdot mL^{-1}$, both samples drop below 80% of metabolic activity of the control. Notably, both random copolymers showed no significant effect on the cellular metabolism of WEHI-164 cells, even at high concentrations of 1000 $\mu g \cdot mL^{-1}$.

For the respective block copolymers, $mPEG_{113}$-*b*-$PMTEGE_{19}$ (14.1 mol %) showed biocompatibility up to 1000 $\mu g \cdot mL^{-1}$ for HEK-293T cells (Figure 10). The incorporation of 26 MTEGE units (18.7 mol %) at concentrations above 75 $\mu g \cdot mL^{-1}$ reduced cellular metabolic activity below the threshold of 80% of the control group. In comparison to HEK-293T, WEHI-164 cells were more sensitive toward the block copolymers.

With respect to envisaged inflammation targeting applications, it is particularly important, to what extent the oxidized products of mPEG-*b*-PMTEGE exert cytotoxic effects. To study this, we investigated the block copolymer with the highest amount of MTEGE. $mPEG_{113}$-*b*-$PMTEGE_{26}$, and its oxidized derivatives showed similar effects on HEK-293T cells as $mPEG_{113}$ itself (Figure 11). Regarding WEHI-164 cells, an inhibition of cellular metabolic activity at high concentrations (1000 $\mu g \cdot mL^{-1}$) was observed for $mPEG_{113}$-*b*-$PMTEGE_{26}$ and its sulfone derivative. In contrast, WEHI-164 cells incubated with $mPEG_{113}$-*b*-$PMSOEGE_{26}$ (sulfoxide units) exceeded 80% of metabolic activity of the control group, even at high concentrations (1000 $\mu g \cdot mL^{-1}$), similar to neat $mPEG_{113}$. To sum up, $mPEG_{113}$-*b*-$PMTEGE_{26}$ and its oxidized derivatives had only marginal effects on the cellular metabolism of HEK-293T and WEHI-164 cells in the range up to 1000 $\mu g \cdot mL^{-1}$, which is key for biomedical applications.

Post-polymerization Modification. To highlight in a comprehensive manner the potential of MTEGE and thioether-functional PEGs, we further demonstrate their use as precursors for highly functional sulfonium structures via click-type alkylation and alkoxylation. Positively charged sulfonium-PEGs are potential candidates for DNA/RNA complexation and represent an interesting polymer class themselves.

Alkylation. In contrast to common ethers, the sulfur in thioethers is nucleophilic and can react with alkyl halides to form sulfonium salts. Recently, Kramer and Deming applied this concept to obtain various highly functional and stable sulfonium derivatives based on poly(L-methionine).[4,20,58] Here, we "quaternized" the MTEGE units of mPEG-*b*-PMTEGE with bromoacetic acid or bromoacetamide to demonstrate their potential as precursors for highly functional sulfur-based polyelectrolytes (Figure 12, left). After modification, FT-IR spectra show new bands, that can be assigned to the carboxyl-group (1620 cm^{-1}) or the amide-group (1682 cm^{-1} (amide I) and 1624 cm^{-1} (amide II)), respectively (Figure 12, right).

Successful modification can also be followed by ^1H and ^{13}C NMR spectroscopy. Figure S31 shows the ^1H NMR spectrum

DOI: 10.1021/jacs.6b04548
J. Am. Chem. Soc. 2016, 138, 9212−9223

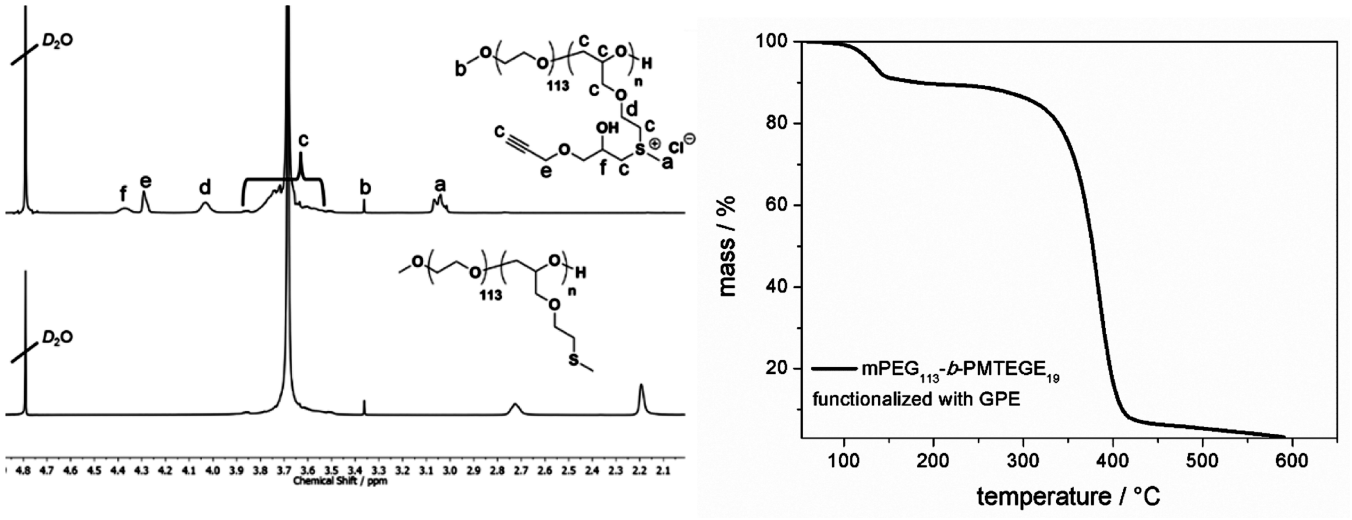

Figure 13. ^{1}H NMR spectra (D_2O, 400 MHz) of $mPEG_{113}$-*b*-$PMTEGE_{19}$ and GPE-functionalized $mPEG_{113}$-*b*-$PMTEGE_{19}$ (left). TGA trace of GPE-functionalized $mPEG_{113}$-*b*-$PMTEGE_{19}$ (right).

of amide-functional mPEG-*b*-PMTEGE. The methyl group at the sulfonium moiety shifted downfield to 3 ppm, and a new resonance at 4 ppm appeared ($-OCH_2CH_2S+$). All other signals overlap with the backbone signal. Further, Figure S32 gives the respective ^{13}C NMR spectra: both carbon atoms next to the sulfur atom shift downfield, and two additional signals occur at 64.9 ppm ($-OCH_2CH_2S+$) and 166.3 ppm ($-CONH_2$). In analogy, the spectrum for carboxyl-functionalized polymer is shown in Figure S33. The introduction of highly polar functional groups further influence the thermal properties of the block copolymers. In DSC measurements, we observe a strong increase in T_g after alkylation (Table S3). We attribute the high T_g's to the introduced charges and the emerging hydrogen bonds between the carboxyl and amide groups, respectively. Interestingly, the T_g of carboxyl-functionalized polymers is higher than the respective amide-functionalized polymers, which is unexpected[59] but might be caused by additional ionic interactions of the acid groups with the charged sulfonium moieties. Furthermore, TGA measurements show that sulfonium-PEG derivatives decompose around temperatures of ∼130 °C (Figure S34). At high temperatures, primarily dealkylation occurs, as deduced from ^{1}H NMR spectra after heating of the samples (not shown). Yet, alkylated mPEG-*b*-PMTEGEs are stable under ambient conditions. The significance of sulfonium polyelectrolytes was demonstrated by Long and co-workers and Matyjaszewski and co-workers, who explored the use of methylated sulfonium poly(methyl)-methacrylates for DNA and siRNA delivery.[21,22] We believe that PEG-based sulfonium derivatives could be suitable alternatives to the above-mentioned polymers, and their complexation and transport efficiencies need to be tested.

Alkoxylation. Recently, Gharakhanian and Deming demonstrated successful functionalization of thioethers with various epoxides as an alternative strategy to their alkylation (Alkylation section).[3] In an analogous manner, we can manipulate the reactivity of MTEGE by pH: at high pH, the nucleophilicity of the sulfide is not sufficient to ring-open an epoxide, and controlled AROP of the monomer can proceed, while at low pH the epoxide is activated and the sulfur(II) species is able to attack the epoxide ring. We studied this concept by addition of epichlorohydrin (ECH) (Figure S35), allyl glycidyl ether (AGE) (Figure S36), and glycidyl propargyl ether (GPE) to mPEG-*b*-PMTEGE block copolymers. Figure 13 illustrates the ^{1}H NMR spectrum of GPE-functionalized mPEG-*b*-PMTEGE.

The methyl-group at the charged sulfur atom shifts from 2.19 to 3.04 ppm, and additional signals at 4.03 ppm ($-OCH_2CH_2S+$), 4.29 ppm ($HC{\equiv}CCH_2-$) and 4.37 ppm ($-CH_2CHOCH_2$) appear. Note that the alkyne proton signal overlaps with the broad polyether backbone signal, which is not uncommon.[60] However, one can detect the characteristic signals of the alkyne group in the FT-IR spectrum (Figure S37). The respective HSQC spectrum of GPE-functionalized PEG−PMTEGE shows signal splitting of signals in close proximity to the sulfur atom (Figure S38). This phenomenon is explained by the use of racemic epoxides. After alkoxylation, a chiral sulfonium center is formed, and detected resonances might depend on the stereo information on the attached epoxide (*R*- vs *S*-). Alkoxylation with optically pure epoxides was not performed.

Similar to the alkylated derivatives, TGA measurements showed dealkylation at 120−130 °C, which is exemplarily shown for GPE functionalized mPEG-*b*-PMTEGE (Figure 13, right). Dealkylation or elimination during workup of the reaction have not been observed. In summary, alkoxylated PEG−PMTEGE copolymers are stable at ambient temperatures similar to the reported alkoxylated poly(L-methionine)[3] and enlarge the toolbox for highly functional sulfonium polyelectrolytes with polar polyether backbone.

■ CONCLUSION

We present a convenient synthesis of a novel epoxide monomer, 2-(methylthio)ethyl glycidyl ether (MTEGE), which can be copolymerized via AROP to yield well-defined thioether-functional PEGs. In a comprehensive study, synthesis and properties of random and block copolymers with PEG have been studied. The statistical copolymerization of MTEGE with EO was monitored via real-time ^{1}H NMR kinetics in DMSO, revealing an ideally random microstructure (r_{EO} = 0.92 ± 0.02, r_{MTEGE} = 1.06 ± 0.02). The random copolymers with 5−24 mol % MTEGE are water-soluble, with tunable cloud points in the range of 28−88 °C. In contrast, DLS studies show that $mPEG_{113}$-*b*-$PMTEGE_n$ block copolymers with $n \geq 9$ form

DOI: 10.1021/jacs.6b04548
J. Am. Chem. Soc. 2016, 138, 9212−9223

defined micelles in water. Notably, disassembly of the micelles occurs when oxidized with 1 wt % H_2O_2, and pure unimers were detected. Hydrogen peroxide oxidizes the nonpolar thioether moieties to more polar sulfoxide groups, leading to a change in the hydrophilic/hydrophobic balance. Fluorescence studies with Nile Red show successful encapsulation and controlled release upon addition of dilute H_2O_2 after 1−2 h, supporting the redox-responsive characteristics of the micellar nanocarriers. The oxidation responsiveness represents the most intriguing feature of the mPEG-*b*-PMTEGE block copolymers and demonstrates their potential for future inflammation targeting. MTT assays employing HEK-293T and WEHI-164 cell lines demonstrated excellent biocompatibility of the thioether-PEGs and their oxidized derivatives.

Further, we demonstrated the use of thioether-PEGs as a precursor for sulfur-based polyelectrolytes. Alkylation and alkoxylation in aqueous solution render multifunctional sulfonium-derivatives bearing carboxyl-, amide-, chloro, allyl-, or propargyl groups. These tertiary sulfonium-PEGs are stable in aqueous solution under ambient temperatures. In conclusion, the presented thioether PEGs with their methionine-like side chain and their derivatives possess potential for a variety of applications, ranging from redox-sensitive nanotransporters and inflammation targeting[12,50,56,61,62] to polyion complexes[21,22] and surface modification.[63−65]

■ ASSOCIATED CONTENT

Supporting Information

The Supporting Information is available free of charge on the ACS Publications website at DOI: 10.1021/jacs.6b04548.

Experimental procedures, additional data, and NMR spectra (PDF)

■ AUTHOR INFORMATION

Corresponding Author

*hfrey@uni-mainz.de

Notes

The authors declare no competing financial interest.

■ ACKNOWLEDGMENTS

J.H. is grateful to the Fonds der Chemischen Industrie for a scholarship and thanks Christian Jochum for technical assistance. J.H. and D.L. acknowledge a fellowship through the Excellence Initiative (DFG/GSC 266) in the context of MAINZ "Materials Science in Mainz". The authors thank Prof. M. Schmidt, Institute of Physical Chemistry, Johannes Gutenberg-University Mainz, for the possibility to use the light scattering facilities. The authors also thank M. Maskos, Fraunhofer ICT-IMM Mainz, for the opportunity to use the CryoTEM. Further, the authors thank Prof. C. Sönnichsen, Institute of Physical Chemistry, and Prof. K. Heinze, Institute of Inorganic Chemisty, Johannes Gutenberg-University Mainz, for the possibility to conduct fluorescence spectroscopy. We acknowledge Evelyn Montermann, Dept. of Dermatology, University Medical Center Mainz, for performing MTT assays.

■ REFERENCES

(1) Vo, C. D.; Kilcher, G.; Tirelli, N. *Macromol. Rapid Commun.* **2009**, *30*, 299−315.
(2) Oae, S. *Organic Chemistry of Sulfur*; Springer US, Boston, MA. 1977.
(3) Gharakhanian, E. G.; Deming, T. J. *Biomacromolecules* **2015**, *16*, 1802−1806.
(4) Kramer, J. R.; Deming, T. J. *Biomacromolecules* **2012**, *13*, 1719−1723.
(5) Batz, H. G.; Hofmann, V.; Ringsdorf, H. *Makromol. Chem.* **1973**, *169*, 323−325.
(6) Hofmann, V.; Ringsdorf, H.; Muacevic, G. *Makromol. Chem.* **1975**, *176*, 1929−1943.
(7) Napoli, A.; Valentini, M.; Tirelli, N.; Müller, M.; Hubbell, J. A. *Nat. Mater.* **2004**, *3*, 183−189.
(8) Napoli, A.; Boerakker, M. J.; Tirelli, N.; Nolte, R. J. M.; Sommerdijk, N. A. J. M; Hubbell, J. A. *Langmuir* **2004**, *20*, 3487−3491.
(9) Napoli, A.; Bermudez, H.; Hubbell, J. A. *Langmuir* **2005**, *21*, 9149−9153.
(10) Wang, L.; Kilcher, G.; Tirelli, N. *Macromol. Biosci.* **2007**, *7*, 987−998.
(11) Carampin, P.; Lallana, E.; Laliturai, J.; Carroccio, S. C.; Puglisi, C.; Tirelli, N. *Macromol. Chem. Phys.* **2012**, *213*, 2052−2061.
(12) Lallana, E.; Tirelli, N. *Macromol. Chem. Phys.* **2013**, *214*, 143−158.
(13) Hu, P.; Tirelli, N. *Bioconjugate Chem.* **2012**, *23*, 438−449.
(14) Fu, X.; Ma, Y.; Shen, Y.; Fu, W.; Li, Z. *Biomacromolecules* **2014**, *15*, 1055−1061.
(15) Jeanmaire, D.; Laliturai, J.; Almalik, A.; Carampin, P.; d'Arcy, R.; Lallana, E.; Evans, R.; Winpenny, R. E. P.; Tirelli, N. *Polym. Chem.* **2014**, *5*, 1393−1404.
(16) d'Arcy, R.; Siani, A.; Lallana, E.; Tirelli, N. *Macromolecules* **2015**, *48*, 8108−8120.
(17) Xiao, C.; Ding, J.; Ma, L.; Yang, C.; Zhuang, X.; Chen, X. *Polym. Chem.* **2015**, *6*, 738−747.
(18) Allen, B. L.; Johnson, J. D.; Walker, J. P. *ACS Nano* **2011**, *5*, 5263−5272.
(19) Wu, W.-X.; Yang, X.-L.; Liu, B.-Y.; Deng, Q.-F.; Xun, M.-M.; Wang, N.; Yu, X.-Q. *RSC Adv.* **2016**, *6*, 11870−11879.
(20) Kramer, J. R.; Deming, T. J. *J. Am. Chem. Soc.* **2014**, *136*, 5547−5550.
(21) Hemp, S. T.; Allen, M. H.; Smith, A. E.; Long, T. E. *ACS Macro Lett.* **2013**, *2*, 731−735.
(22) Mackenzie, M. C.; Shrivats, A. R.; Konkolewicz, D.; Averick, S. E.; McDermott, M. C.; Hollinger, J. O.; Matyjaszewski, K. *Biomacromolecules* **2015**, *16*, 236−245.
(23) Herzberger, J.; Niederer, K.; Pohlit, H.; Seiwert, J.; Worm, M.; Wurm, F. R.; Frey, H. *Chem. Rev.* **2016**, *116*, 2170−2243.
(24) Lee, J. C.; Litt, M. H.; Rogers, C. E. *Macromolecules* **1997**, *30*, 3766−3774.
(25) Lee, A.; Lundberg, P.; Klinger, D.; Lee, B. F.; Hawker, C. J.; Lynd, N. A. *Polym. Chem.* **2013**, *4*, 5735−5742.
(26) Hans, M.; Keul, H.; Moeller, M. *Polymer* **2009**, *50*, 1103−1108.
(27) Mangold, C.; Dingels, C.; Obermeier, B.; Frey, H.; Wurm, F. *Macromolecules* **2011**, *44*, 6326−6334.
(28) Herzberger, J.; Kurzbach, D.; Werre, M.; Fischer, K.; Hinderberger, D.; Frey, H. *Macromolecules* **2014**, *47*, 7679−7690.
(29) Niederer, K.; Schüll, C.; Leibig, D.; Johann, T.; Frey, H. *Macromolecules* **2016**, *49*, 1655−1665.
(30) Beckingham, B. S.; Sanoja, G. E.; Lynd, N. A. *Macromolecules* **2015**, *48*, 6922−6930.
(31) Lee, B. F.; Wolffs, M.; Delaney, K. T.; Sprafke, J. K.; Leibfarth, F. A.; Hawker, C. J.; Lynd, N. A. *Macromolecules* **2012**, *45*, 3722−3731.
(32) Fuller, C. S. *Chem. Rev.* **1940**, *26*, 143−167.
(33) Brandrup, J.; Immergut, E. H.; Grulke, E. A. *Polymer handbook*, 4th ed.; Wiley: New York, Chichester, 2004.
(34) Müller, S. S.; Moers, C.; Frey, H. *Macromolecules* **2014**, *47*, 5492−5500.
(35) Mangold, C.; Obermeier, B.; Wurm, F.; Frey, H. *Macromol. Rapid Commun.* **2011**, *32*, 1930−1934.
(36) Shikata, T.; Okuzono, M.; Sugimoto, N. *Macromolecules* **2013**, *46*, 1956−1961.

DOI: 10.1021/jacs.6b04548
J. Am. Chem. Soc. 2016, 138, 9212−9223

(37) Derici, L.; Ledger, S.; Mai, S.-M.; Booth, C.; Hamley, I. W.; Skov Pedersen, J. *Phys. Chem. Chem. Phys.* **1999**, *1*, 2773−2785.
(38) Topp, M. D. C.; Dijkstra, P. J.; Talsma, H.; Feijen, H. *Macromolecules* **1997**, *30*, 8518−8520.
(39) Kjøniksen, A.-L.; Nyström, B.; Tenhu, H. *Colloids Surf., A* **2003**, *228*, 75−83.
(40) Motokawa, R.; Morishita, K.; Koizumi, S.; Nakahira, T.; Annaka, M. *Macromolecules* **2005**, *38*, 5748−5760.
(41) Yan, J.; Ji, W.; Chen, E.; Li, Z.; Liang, D. *Macromolecules* **2008**, *41*, 4908−4913.
(42) Huang, X.; Du, F.; Cheng, J.; Dong, Y.; Liang, D.; Ji, S.; Lin, S.-S.; Li, Z. *Macromolecules* **2009**, *42*, 783−790.
(43) Kurzbach, D.; Wilms, V. S.; Frey, H.; Hinderberger, D. *ACS Macro Lett.* **2013**, *2*, 128−131.
(44) Kelarakis, A.; Havredaki, V.; Yu, G.-E.; Derici, L.; Booth, C. *Macromolecules* **1998**, *31*, 944−946.
(45) Bedells, A. D.; Arafeh, R. M.; Yang, Z.; Attwood, D.; Heatley, F.; Padget, J. C.; Price, C.; Booth, C. *J. Chem. Soc., Faraday Trans.* **1993**, *89*, 1235−1242.
(46) Wilhelm, M.; Zhao, C. L.; Wang, Y.; Xu, R.; Winnik, M. A.; Mura, J. L.; Riess, G.; Croucher, M. D. *Macromolecules* **1991**, *24*, 1033−1040.
(47) Yasugi, K.; Nagasaki, Y.; Kato, M.; Kataoka, K. *J. Controlled Release* **1999**, *62*, 89−100.
(48) Stauch, O.; Schubert, R.; Savin, G.; Burchard, W. *Biomacromolecules* **2002**, *3*, 565−578.
(49) Förster, S.; Zisenis, M.; Wenz, E.; Antonietti, M. *J. Chem. Phys.* **1996**, *104*, 9956−9970.
(50) d'Arcy, R.; Tirelli, N. *Polym. Adv. Technol.* **2014**, *25*, 478−498.
(51) Covington, A. K.; Paabo, M.; Robinson, R. A.; Bates, R. G. *Anal. Chem.* **1968**, *40*, 700−706.
(52) Sarapas, J. M.; Tew, G. N. *Macromolecules* **2016**, *49*, 1154−1162.
(53) Zhang, M.; Song, C.-C.; Ji, R.; Qiao, Z.-Y.; Yang, C.; Qiu, F.-Y.; Liang, D.-H.; Du, F.-S.; Li, Z.-C. *Polym. Chem.* **2016**, *7*, 1494−1504.
(54) Brubaker, C. E.; Velluto, D.; Demurtas, D.; Phelps, E. A.; Hubbell, J. A. *ACS Nano* **2015**, *9*, 6872−6881.
(55) de Gracia Lux, C.; Joshi-Barr, S.; Nguyen, T.; Mahmoud, E.; Schopf, E.; Fomina, N.; Almutairi, A. *J. Am. Chem. Soc.* **2012**, *134*, 15758−15764.
(56) Xu, Q.; He, C.; Xiao, C.; Chen, X. *Macromol. Biosci.* **2016**, *16*, 635−646.
(57) Fruijtier-Pölloth, C. *Toxicology* **2005**, *214*, 1−38.
(58) Kramer, J. R.; Deming, T. J. *Chem. Commun.* **2013**, *49*, 5144−5146.
(59) Herzberger, J.; Frey, H. *Macromolecules* **2015**, *48*, 8144−8153.
(60) Thomas, A.; Niederer, K.; Wurm, F.; Frey, H. *Polym. Chem.* **2014**, *5*, 899−909.
(61) Song, C.-C.; Du, F.-S.; Li, Z.-C. *J. Mater. Chem. B* **2014**, *2*, 3413−3426.
(62) Tapeinos, C.; Pandit, A. *Adv. Mater.* **2016**, DOI: 10.1002/adma.201505376.
(63) Stouffer, J. M.; McCarthy, T. J. *Macromolecules* **1988**, *21*, 1204−1208.
(64) Lenk, T. J.; Hallmark, V. M.; Rabolt, J. F.; Haeussling, L.; Ringsdorf, H. *Macromolecules* **1993**, *26*, 1230−1237.
(65) Fujii, S.; McCarthy, T. J. *Langmuir* **2016**, *32*, 765−771.

DOI: 10.1021/jacs.6b04548
J. Am. Chem. Soc. 2016, 138, 9212−9223